PAPER

Check for updates

Terpenes, natural dyes and photochemistry: toward the synthesis of photoactive bio-based materials with biocide properties†

Louise Breloy,[a] Christine Elian, [ID] [a] Vanessa Alphonse,[b] Sonia Lajnef,[c] Fabienne Peyrot,[c,d] Denis Jacquemin, [ID] [e,f] Simon Pascal, [ID] [e] Enguerran Devernois,[g] Thibaud Coradin, [ID] [g] Samir Abbad Andaloussi[b] and Davy-Louis Versace [ID] *[a]

Combining bioresources and photo-induced polymerization is a promising way to design sustainable and high-performing antibacterial materials. In this study, we propose a green synthesis of bio-based materials with dual anti-bacterial properties by photopolymerization. Two new methacrylate-based hydroxyanthraquinones derived from purpurin and alizarin (P-3Ac and Al-2Ac) have been designed to promote the polymerization of bio-based vegetable oil and terpene blend mixtures under visible-light irradiation up to 470 nm. All the photochemical mechanisms involved in the photopolymerization processes have been described by steady state photolysis, electron spin resonance spin-trapping (ESR ST) and real-time Fourier transform infrared (RT-FTIR) spectroscopy. Interestingly, the photo-initiating properties of P-3Ac and Al-2Ac are greatly enhanced in comparison with the native unmodified purpurin and alizarin. Polymerization of soybean oil acrylate and linalool through a thiol–ene process has led to the formation of photoactive bio-based materials able to generate biocide reactive oxygen species (ROS) upon light exposure which can also be used as contact-killing materials for tremendous inhibition of bacterial growth. The respective effects of each biocide agent (ROS and linalool) were compared and combined, highlighting stunning inhibition properties of the materials (higher than 99.99%) against both *E. coli* (Gram negative) and *S. aureus* (Gram positive), even after a second antibacterial recycling test. Prior to photo-printing experiments, rheological studies have been performed to design greener 3D-photoinduced materials. According to the high bio-renewable carbon contents of the photosensitive P-3Ac-based formulation and its great processability, 3D objects have been designed using Digital Light Processing (DLP) technology upon 405 nm light emitting diode exposure.

[a]Univ Paris Est Creteil, CNRS, ICMPE, UMR 7182, 2 rue Henri Dunant, 94320 Thiais, France. E-mail: davy-louis.versace@u-pec.fr
[b]Laboratoire Eau, Environnement, Systemes Urbains (LEESU), UMR-MA 102, Universite Paris-Est Creteil (UPEC), 61 Avenue Genéral de Gaulle, 94010 Créteil Cedex, France
[c]Université Paris Cité, CNRS, Laboratoire de Chimie et Biochimie Pharmacologiques et Toxicologiques, F-75006 Paris, France
[d]Sorbonne-Université, Institut National Supérieur du Professorat et de l'Education (INSPE) de l'académie de Paris, F-75016 Paris, France
[e]Nantes Université, CNRS, CEISAM, UMR 6230, F-44000 Nantes, France
[f]Institut Universitaire de France (IUF), F-75005 Paris, France
[g]Sorbonne Université-CNRS, Laboratoire de Chimie de la Matière Condensée de Paris, F-75005 Paris, France

†Electronic supplementary information (ESI) available: ^{1}H NMR, ^{13}C NMR, and IR spectra of P-3Ac and Al-2Ac; steady-state photolysis of P-3Ac and Al-2Ac-based photoinitiating systems; experimental and simulated ESR spectra obtained from the photolysis of Al-2Ac/TT/DMPO solutions; additional kinetic profiles of acrylate and thiol conversions; optical images of Al-2Ac and P-3Ac based pellets; evolution of the colony forming units (CFUs) of *S. aureus* and *E. coli* at the surface of the P-3Ac/TT/SOA and P-3Ac/TT/Lin/SOA materials; evolution of viscosity over shear rate and evolution of viscosity over temperature for TT25%/Lin25%/SOA50% and TT25%/SOA75% formulations; antibacterial tests in solutions; cell attachment and metabolic activity assays. See DOI: https://doi.org/10.1039/d4lp00271g

Introduction

The polymer field has become a focal point in addressing current sustainability concerns. Although the production of bio-based polymers significantly increased over the last few decades, their proportion remains lower than that of petro-sourced products (around 3% in 2020).[1] Besides, efforts toward green polymer chemistry are not restricted to the valorisation of bio-resources; production processes need to be rethought according to the principles of green chemistry. In this respect, light-activable bulk polymerization satisfies several criteria compared to classical thermal synthesis.[2,3] Photoinitiated reactions occur in a few minutes, at room temperature and without any solvent, thus preventing the release of volatile organic compounds.[4] The current replacement of UV emitting lamps by visible light emitting diodes (LEDs) provides both energy savings and handling safety.[5] Another striking advantage of photopolymerization is spatio-temporal control, allowing appealing applications such as the design of complex microstructures by 3D photo-printing.[6,7] However, the

current photopolymerizable formulations suffer from high prices and a lack of sustainability.

Yet, many bio-based monomers were proved perfectly adapted to the photopolymerization process. Among them, vegetable oils,[8–12] phenolic compounds[13–17] and terpenes[18–21] attracted much attention because of their low price and abundance. Their functional groups, *i.e.* alcohol, phenol or vinyl, facilitate their transformation into monomers for thiol–ene, cationic (CP) or free-radical polymerizations (FRP).[3,22–24] However, most of the examples proposed in the literature concerning photopolymerization of bio-based monomers rely on UV initiation.[8,25] Besides, the intrinsic properties of each monomer may limit their processability, notably for 3D-photoprinting. For instance, vegetable oil derivatives are highly viscous,[13] while terpenes generally have too low viscosities to form materials.[21] Several alternatives, such as the dilution of vegetable oils with solvent,[26] synthetic[27] or bio-based diluents,[13,27] or the pre-polymerization of terpenes before photo-crosslinking[21,28] have been suggested.

Meanwhile, increasing interest in the development of bio-based photo-initiators (PIs)[29–31] came to the forefront. Indeed, visible-light photopolymerization can efficiently occur in the presence of natural dyes.[29] The fewer chemical modifications the natural compound undergoes, the lower the environmental impact. Many works were dedicated to quinone derivatives,[32,33] especially hydroxyanthraquinones,[34–37] which are used as Norrish Type II photo-initiators. However, previous investigations on native hydroxyanthraquinones reported that their capability to initiate FRP is limited, probably due to the radical scavenging effects of phenol groups.[36,37] It has recently been demonstrated that the functionalization of some hydroxyanthraquinones with photopolymerizable groups could considerably enhance their initiating properties while preventing their leakage.[34,35] Notably, the study of quinizarin derivatives emphasized low migration in polymer networks generated by FRP.[38] However, quinizarin is poorly available from natural sources and only found in its glycosylated form. In contrast, alizarin and purpurin constitute, respectively, 7.9% and 1% of madder root composition[39] and can be easily extracted using green solvents such as water or ethanol.[40]

The design of high-performing antibacterial materials has also been a burning topic for decades. Indeed, the medical field faces a high number of hospital-acquired infections (HAIs) due to bacterial proliferation on surfaces. The number of deaths caused each year by HAIs is worryingly increasing due to the emergence of multi-resistant bacterial strains.[41] Interestingly, the combination of bioresources and photo-induced polymerization offers promising opportunities for the design of safe and green antibacterial materials.[42–44] As previously demonstrated,[31,45–48] some synthetic or natural dyes could play a dual role as visible-light photosensitizers for photopolymerization and as photo-activable antibacterial agents, leading to intrinsically antibacterial materials.[44] Also, some natural monomers show intrinsic antibacterial properties even after their introduction into the polymer network.[49] For instance, eugenol[50,51] and linalool,[52,53] isolated from clove and lavender essential oils, respectively, demonstrate this effect.

The originality of this study is to associate the antibacterial properties of photoreactive bio-based monomers using essential oils with the method of photodynamic inactivation of bacteria through the thiol–ene process. To the best of our knowledge and despite significant advances in the design of new antibacterial materials, our strategy has never been described yet. This prompted us to design efficient 2D and 3D bio-based antibacterial materials using linalool as an antibacterial monomer, soybean oil acrylate (SOA) as a crosslinker, and natural dye derivatives as photosensitizers for visible light-induced polymerization and as generators of biocide agents. Final materials were obtained under visible-light irradiation, using natural dyes extracted from madder root, *i.e.* alizarin and purpurin.[39,54] Particular attention was paid to the photochemical mechanisms involved during the irradiation of the alizarin and purpurin derivatives by steady-state photolysis and ESR ST experiments. Several photosensitive bio-based formulations containing linalool (or geraniol, myrcene, and farnesene), SOA and purpurin (or alizarin) derivatives were studied, and their reactivity under LEDs@405, 455 and 470 nm irradiation was monitored by real-time infrared (RT-FTIR) spectroscopy. The design of the final materials was done by polymerization of linalool with SOA by combining the thiol–ene process and free-radical polymerization. The anti-adhesion properties of the photoinduced materials were evaluated against *Escherichia coli* (*E. coli*, Gram-negative bacteria) and *Staphylococcus aureus* (*S. aureus*, Gram-positive bacteria), and the respective antibacterial effects of linalool and light-induced ROS on bacterial adhesion were compared. Finally, rheological studies allowed us to enhance the processability of photosensitive formulations (linalool/SOA/thiol derivative/purpurin derived dye) for 3D-printing experiments under visible-light irradiation with Digital Light Processing (DLP) technology.

Experimental

Materials

Alizarin (Al), purpurin (Pur), dimethylaminopyridine (DMAP), methacrylic anhydride, trimethylolpropane tris(3-mercaptopropionate) (TT, ≥95%), 1,3-diphenyliso-benzofurane (DPBF), nitroblue tetrazolium chloride (NB), soybean oil acrylate (SOA), linalool (Lin, 97%), geraniol (Ger, 98%), myrcene (Myr) and farnesene (Far) were provided by Sigma-Aldrich. 9,10-Anthraquinone (AQ) was supplied by Alfa Aesar. 5,5-Dimethyl-1-pyrroline *N*-oxide (DMPO) was supplied by Sigma-Aldrich and used as the spin trapping agent. All chemical structures of the compounds are reported in Table 1.

Synthesis of di-methacrylated alizarin (Al-2Ac)

0.5 g of alizarin (2.1 mmol) and 512 mg of DMAP (1 eq. to –OH) were dissolved in 25 mL of dry acetone. The medium was stirred for 1 h under continuous argon flux. Afterwards, 1.25 mL of methacrylic anhydride (2 eq. to –OH) was added dropwise and the mixture was stirred at room temperature. After 8 h, an additional 0.62 mL (1 eq. to –OH) of anhydride

© 2025 The Author(s). Published by the Royal Society of Chemistry

RSC Appl. Polym., 2025, **3**, 222–237 | **223**

Table 1 Structures and roles of the different chemical compounds used in this study

Name	Structure	Role
9,10-Anthraquinone (AQ)		Photo-sensitizer (PS)
Alizarin (Al)		PS
Purpurin (P)		PS
Di-methacrylated alizarin (Al-2Ac)		PS
Tri-methacrylated purpurin (P-3Ac)		PS
Linalool (Lin)		Monomer and antibacterial agent
Geraniol (Ger)		Monomer and antibacterial agent
Myrcene (Myr)		Monomer and antibacterial agent
Farnesene (Far)		Monomer and antibacterial agent
Soybean oil acrylate (SOA)		Monomer

Table 1 *(Contd.)*

Name	Structure	Role
Trimethylolpropane tris(3-mercaptopropionate) (TT)		Co-initiator and cross-linker
DMPO		Spin trap
1,3-Diphenylisobenzofurane (DPBF)		Singlet oxygen trap
p-Nitroblue tetrazolium chloride (NB)		Superoxide anion trap

methacrylate was introduced and stirring was continued over 2 days. Acetone was evaporated, and the raw product was directly purified by flash chromatography (isocratic mode, cyclohexane/ethyl acetate 95/5). A pale-yellow powder corresponding to Al-2Ac was collected (88% yield). TLC (cyclohexane/ethyl acetate 80/20): R_f = 0.26. **NMR ^{1}H** (CDCl$_3$, 400 MHz), δ (ppm): 2.01 (s, 3H, Ha′), 2.10 (s, 3H, Ha), 5.79 (s, 1H, Hc′), 5.83 (s, 1H, Hc), 6.33 (s, 1H, Hb′), 6.40 (s, 1H, Hb), 7.67 (d, 1H, J = 8.5 Hz, Hd), 7.72–7.75 (m, 2H, Hf and Hi), 8.16 (m, 1H, Hg), 8.22 (m, 1H, Hh), 8.31 (d, 1H, J = 8.5 Hz, He). **NMR ^{13}C** (CDCl$_3$, 100 MHz), δ (ppm): 18.32 (Cd′), 18.49 (Cd), 18.59 (Cg), 126.39 (Ch), 126.72 (Ck′), 127.10 (Ck), 127.38 (Cf), 128.36 (Cc′), 128.65 (Cc), 128.84 (Ch′), 132.25 (Cl′), 132.63 (Cl), 134.18 (Cj′), 134.41 (Cj), 134.86 (Cb′), 135.21 (Cb), 142.35 (Ce′), 148.95 (Ce), 164.29 (Ca′), 164.65 (Ca), 181.48 (Ci′), 181.86 (Ci). **IR** (neat, cm^{-1}): 1755 ($\nu_{CH_2=CCH_3COOR}$), 1672 ($\nu_{C=C}$ of the acrylate group), 1636 ($\nu_{C=O}$ of anthraquinone), 1315 ($\nu_{Ar-O-CO}$) (Fig. S1†).

Synthesis of tri-methacrylate purpurin (P-3Ac)

0.1 g of purpurin (0.39 mmol) and 0.14 g of DMAP (1 eq. to –OH) were dissolved in 25 mL of dry chloroform. The medium was stirred for 1 h under continuous argon flux at room temperature. Afterwards, 0.35 mL of methacrylic anhydride (2 eq. to –OH) was added dropwise and stirring was continued for 8 h. Then, an additional 0.17 mL (1 eq. of –OH) of anhydride methacrylate was added to the mixture, the stirring of which was continued overnight. Chloroform was evaporated, and the raw product was directly purified by flash chromatography (isocratic mode, cyclohexane/ethyl acetate 95/5). A pale-orange powder corresponding to P-3Ac was collected (48% yield). TLC (cyclohexane/ethyl acetate 80/20): R_f = 0.44. **NMR ^{1}H** (CDCl$_3$, 400 MHz), δ (ppm): 2.01 (s, 3H, Ha′), 2.11 (s, 3H, Ha), 2.15 (s, 3H, Ha″), 5.80 (s, 1H, Hc′), 5.84 (s, 1H, Hc), 5.87 (s, 1H, Hc″), 6.32 (s, 1H, Hb′), 6.40 (s, 1H, Hb), 6.45 (s, 1H, Hb″), 7.49 (s, 1H, Hd), 7.72 (m, 2H, He), 8.15 (m, 2H, Hf). **NMR ^{13}C** (CDCl$_3$, 100 MHz), δ (ppm): 18.31 (Cd′), 18.54 (Cd), 18.59 (Cd″), 123.73 (Cf), 124.90 (Ch′), 127.07 (Ch), 127.15 (Ck′), 127.69 (Ck), 128.42 (Cc′), 128.51 (Cc), 129.19 (Cc″), 133.45 (Cl′), 133.48 (Cl), 134.15 (Cj′), 134.31 (Cj), 134.74 (Cb′), 135.17 (Cb), 135.59 (Cb″), 140.69 (Ce′), 148.91 (Ce), 148.97 (Ce″), 163.84 (Ca′), 164.59 (Ca), 165.45 (Ca″), 180.93 (Ci′), 180.37 (Ci). **IR** (neat, cm^{-1}): 1737 ($\nu_{CH_2=CCH_3COOR}$), 1674 ($\nu_{C=C}$ of the acrylate group), 1637 ($\nu_{C=O}$ of anthraquinone), 1292 ($\nu_{Ar-O-CO}$) (Fig. S2†).

© 2025 The Author(s). Published by the Royal Society of Chemistry

RSC Appl. Polym., 2025, **3**, 222–237 | **225**

NMR and IR spectroscopy

^{1}H and ^{13}C NMR spectra were recorded with a Bruker Avance II instrument at 400 MHz and 100 MHz, respectively. A PerkinElmer FT-IR spectrometer was used to record IR spectra between 400 and 4000 cm^{-1}.

UV-visible spectroscopy

A PerkinElmer Lambda 2 spectrophotometer was used to collect absorption spectra between 200 nm and 800 nm.

Molecular modelling

Selected systems were modelled with Gaussian 16.A.03[55] using the DFT PBE0[56]/6-31G(d) approach. All systems were fully optimized without symmetry constraints and analytical frequency calculations were performed to ensure the stability (no imaginary frequency) of all compounds. The open-shell forms were computed using U-DFT. We used a tight optimization criterion, set the SCF convergence to 10^{-10} au, applied the so-called *superfine* integration grid, and set the integral accuracy parameter to 10^{-14} au.

Steady-state photolysis

Al-2Ac and P-3Ac were dissolved in ACN ([Al-2Ac] = 1.4×10^{-4} M and [Pur-3Ac] = 1.2×10^{-4} M), and solutions were irradiated in a quartz cell (1 cm width) upon LED@405 nm irradiation (60 mW cm^{-2}). Experiments were carried out with and without TT ([TT] = 2.4×10^{-3} M).

Photopolymerization kinetic studies

The compositions of all the photosensitive formulations are detailed in the corresponding figure captions. Solutions were spread on a BaF$_2$ pellet with a controlled thickness of 12 μm and irradiated under different LED sources (LED@405 nm–60 mW cm^{-2}, LED@455nm–38 mW cm^{-2} or LED@470 nm–25 mW cm^{-2}) at room temperature under air or in laminate. Kinetic profiles were recorded by real-time Fourier transform infrared (RT-FTIR) spectroscopy using a JASCO FTIR 4700 instrument. The consumption of each monomer functional group was evaluated by RT-FTIR at different wavenumbers, *i.e.* acrylate groups of TMPTA (1636 cm^{-1}) and SOA (1636 cm^{-1} alone and 810 cm^{-1} when mixed with linalool), the thiol group of TT (2570 cm^{-1}), the ene group of linalool (1640 cm^{-1} alone, and 3080 cm^{-1} when mixed with SOA), geraniol (1665 cm^{-1}), farnesene (1590 cm^{-1}) and myrcene (1597 cm^{-1}). IR spectra of TT, Lin, SOA and Ger are described in Fig. S3.†

Irradiation sources. LED@405 nm (60 mW cm^{-2}), LED@455 nm (40 mW cm^{-2}), LED@470 nm (25 mW cm^{-2}) and a xenon lamp (Lightningcure LC8-03, 200 W, 10 mW cm^{-2}) were provided by Thorlabs and Hamamatsu, respectively.

Electron spin resonance spin-trapping (ESR ST)

The samples were prepared by mixing indicated reagents in dry dichloromethane (DCM) in a 4 mm quartz ESR tube, oxygen was removed by argon bubbling through the solution for one minute, and the tube was sealed with a septum cap. DMPO was used as a spin trapping agent. The solutions were analyzed by ESR before and after irradiation outside the ESR resonator using a LED@405 nm source as indicated in the figure caption. ESR measurements were performed using an Elexsys E500 ESR spectrometer (Bruker, Wissembourg, France), operating at the X-band (9.8 GHz) and equipped with an SHQ high-sensitivity cavity. The typical settings used were: microwave power, 10 mW; modulation frequency, 100 kHz; modulation amplitude, 0.05 mT; receiver gain, 60 dB; time constant, 10.24 ms; conversion time, 40.96 ms; datapoints, 1024; sweep width, 7 mT; sweep time, 41.94 s. 20 ESR spectra were recorded sequentially at 21 °C. Figures present the sum of 5 experimental spectra. Data acquisition and processing were performed using Bruker Xepr software. The simulated spectra were recorded with the EasySpin toolbox working on the MATLAB platform.[57]

Preparation of pellets. P-3Ac/TT25%/SOA75% and P-3Ac/TT25%/Lin25%/SOA50% formulations were poured into a round silicon mold (15 mm diameter and 1.3 mm thickness) covered with a polypropylene film to prevent oxygen inhibition. Samples were irradiated for 10 min on each side under LED@405nm (60 mW cm^{-2}) irradiation.

Detection of singlet oxygen

DPBF was used as a singlet oxygen trap. To compare the singlet oxygen production of several photosensitizers (P-3Ac and Al-2Ac), solutions containing 0.03 mM of DPBF and 0.3 mM of each photosensitizer were used. Also, the production of singlet oxygen by the (P-3Ac/TT/SOA) and (P-3Ac/TT/Lin/SOA) pellets that were immersed in 1.5 mL of a methanolic solution of DPBF was measured. All the solid samples were irradiated with a xenon lamp (10 mW cm^{-2}). The photobleaching of DPBF, which is observable through the decrease of its absorbance at 410 nm, was monitored by UV-visible spectroscopy. Blank experiments were also carried out without any photosensitizer or pellet.

Detection of superoxide ions

NB was used as an ion superoxide trap. Photosensitizers alone (P-3Ac and Al-2Ac) and (P-3Ac/TT/SOA) or (P-3Ac/TT/Lin/SOA) pellets were introduced into 1.5 mL of a methanolic solution of NB (0.9 mM). All the photosensitizers or solid samples were irradiated with a xenon lamp (15 mW cm^{-2}). The production of the reduced form of NB, which is easily observable through the increase of the absorbance at 510 nm, was monitored by UV-visible spectroscopy. Blank experiments were also carried out without the addition of photosensitizers or pellets.

Anti-adhesion assay

The capability of P-3Ac/TT/SOA and P-3Ac/TT/Lin/SOA solid pellets to prevent adhesion of bacteria was evaluated against *S. aureus* (ATCC6538) and *E. coli* (ATCC25922). Pellets were immersed in bacterial solution (10^6 CFU mL^{-1}) for 24 h at 37 °C to allow bacterial adhesion on their surface. Then, half of the pellets were put under a solar emission lamp for 1 h on

each side, while the other half remained in the dark. Bacteria were collected at the surface of each pellet according to a previously described method,[35] and colony forming units (CFUs) were counted after 48 h. Experiments were done in triplicate.

Antibacterial tests in solution

The toxicity tests of P-3Ac were performed against two model bacteria, namely *Staphylococcus aureus* ATCC6538 (*S. aureus*, Gram-positive bacteria) and *Escherichia coli* ATCC25922 (*E. coli*, Gram-negative bacteria). First, bacterial preculture was grown for 12 h at 37 °C and aerobically in Luria–Miller medium (LB, Roth). For the antibacterial tests, 96 microplates (which possess a volume of 200 μL each) were filled with a mixture of a suspension of bacteria (four replicates per test) and different concentrations of P-3Ac ranging from 0 to 0.30 mg mL^{-1} were used (for higher concentrations, the precipitation of P-3Ac in the suspension of bacteria was observed). The initial optical density (OD) of the bacteria was 0.05 (read at 600 nm).

Several controls were carried out: abiotic control (without bacteria but with P-3Ac) and biotic control (without P-3Ac but with bacteria). The OD of bacterial suspensions was read periodically at 600 nm to follow bacterial growth for 10 h (MultiSkan SkyHigh, Thermo Scientific). To estimate the percentage of bacterial inhibition, the following equation was used:

$$I(\%) = \text{percentage inhibition}$$
$$= 100 - ((OD_{sample}/OD_{ref}) \times 100)$$

OD$_{ref}$ and OD$_{sample}$ correspond to the optical density (OD) of the reference (bacterial suspension alone in culture media) and the sample (bacterial suspension with P-3Ac), respectively.

Cell attachment and metabolic activity assays

Normal human dermal fibroblasts (NHDFs) were used from passages 4 to 7. Cells were cultured in a 5% CO$_2$ humidified incubator (Thermo Scientific) and the medium (DMEM 1×, 10% v/v of foetal bovine serum, 1% penicillin/streptomycin and 1% fungizone) was changed every 3 days. Disks (*n* = 3) of the P-3Ac/TT25%/Lin25%/SOA50% material were placed in a 24-well plate and 0.5 mL of a NHDF suspension at a density of 100 000 cells per mL was deposited on their surface. Controls were prepared by seeding NHDFs at the same cell density in disk-free wells (*n* = 3). The samples were placed in a 5% CO$_2$ humidified incubator and cultured for 24 h.

Cellular metabolic activity was assessed by alamarBlue after 24 h. The medium was removed and replaced with a complete medium without phenol red. Fresh medium with 10% (v/v) alamarBlue reagent was put in contact with gels for 4 h. After the colour change, it was removed, and the absorbance of the supernatant was measured at 570 nm and 600 nm. The reduction percentage was calculated according to the supplier's recommendations. Cells were fixed with 4% PFA, permeabilized using PBS – 0.2% Triton and stained with phalloidin (1/200 dilution in PBS) and DAPI (1/5000 dilution in PBS). Phalloidin stains the actin filament in cell cytoskeletons and

DAPI stains cell nuclei. Samples were observed with an Upright Leica confocal scanning microscope.

Water contact angle

A KRÜSS EasyDrop goniometer instrument was used to measure the water contact angle at room temperature. 20 μL of water were dropped on the surface of the photoinduced materials. Drop Shape Analysis System software allows us to evaluate the hydrophily/hydrophobicity of the surface of each sample. Measurements were repeated five times for each material.

Rheology

Rheology experiments were carried out with TT25%/Lin25%/SOA50% and TT25%/SOA75% formulations using a TA Instruments rheometer (AR 1000) in parallel plate mode (20 mm diameter). A shear rate ramp was performed at either 25 °C or 50 °C between 0.1 and 950 s^{-1}. The temperature ramp was applied at a constant shear of 1 s^{-1} between 25 °C and 50 °C with a 2 °C min^{-1} ramp.

3D-photoprinting experiments

3D objects were designed from the photosensitive formulation TT/Lin/SOA (25%/25%/50% w/w) with P-3Ac (0.5 wt%), by using an Asiga PICO 2 DLP printer with a nominal XY resolution of 39 μm and a diode as the light-emitting source (405 nm; light intensity = 17.30 mW cm^{-2}). The printing parameters were experimentally set as follows for the "star" object: layer thickness, 50 μm and layer exposure time, 29.864 s.

Results and discussion

Synthesis of methacrylated derivatives of purpurin and alizarin

Although the functionalization of phenols with methacrylate groups is most of the time carried out using hazardous methacryloyl chloride, safer alternatives have been now proposed.[58] Alizarin and purpurin-based methacrylate photosensitizers were synthesized by means of an esterification reaction between alizarin (or purpurin) and methacrylic anhydride with DMAP in acetone (or chloroform), respectively, with a reflux step at 60 °C.[38] The transesterification mechanism in the case of alizarin is shown in Scheme S1.† Al-2Ac and P-3Ac were successfully obtained with 88% and 48% yields, respectively (Scheme S2†). The chemical structure of both photosensitizers was confirmed by NMR and IR spectroscopy (Fig. S1 and S2†). Notably, the ^{1}H NMR signals of the methacrylate protons are observed at 5.8 and 6.4 ppm, and the IR absorption bands corresponding to C=C stretching vibration were observed at ~1670 cm^{-1}.

Photochemical reactivity of Al-2Ac (or P-3Ac) alone and in the presence of a thiol crosslinker (TT)

The absorption spectra of Al-2Ac and P-3Ac are superimposed with those of Al, Pur and AQ, as shown in Fig. 1. In native alizarin and purpurin, a $^1(\pi–\pi^*)$ charge transfer transition due to
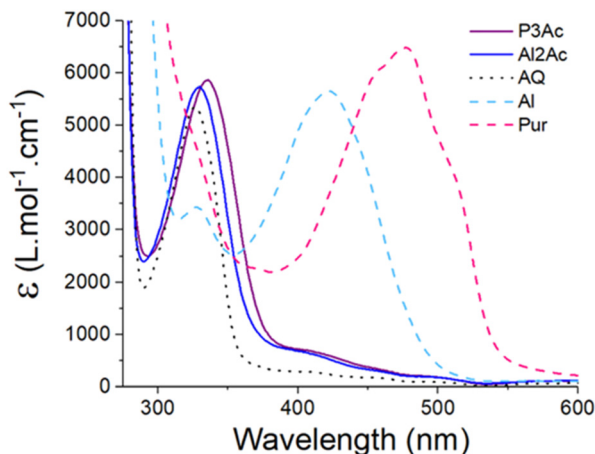
© 2025 The Author(s). Published by the Royal Society of Chemistry

RSC Appl. Polym., 2025, **3**, 222–237 | **227**

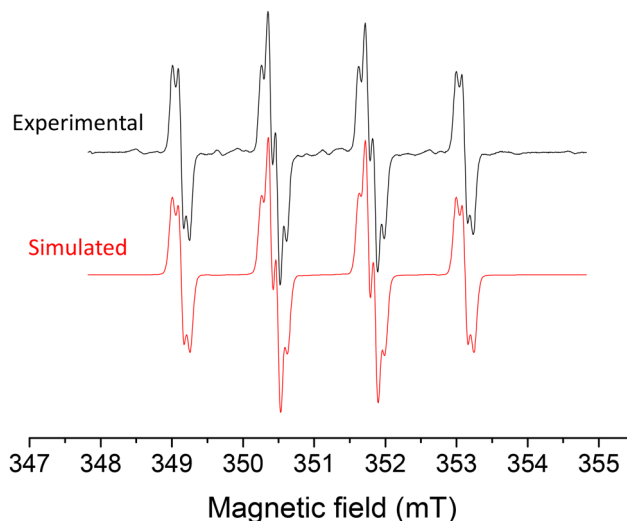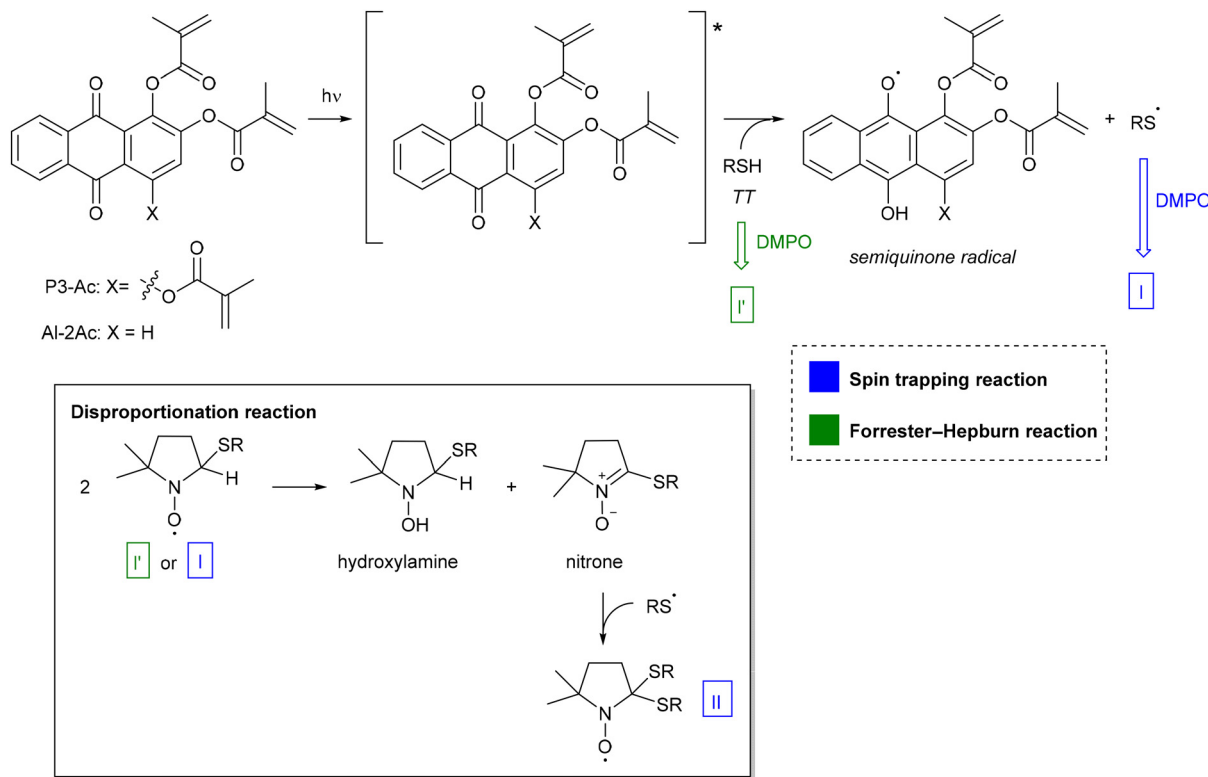Fig. 1 Absorption spectra of P-3Ac, Al-2Ac, AQ, Al and Pur in ACN.

Fig. 2 The normalized experimental and simulated ESR ST spectra obtained in DCM under argon during 120 s *ex situ* LED@405 nm irradiation of P-3Ac/TT/DMPO. Intensity of irradiation = 60 mW cm^{-2}. Only one species (I, Scheme 1) was considered in the simulation.

the electron-donor effect of phenol groups is responsible for the absorption band in the visible range.[59] However, by functionalizing alizarin and purpurin with electron withdrawing groups (methacrylate function), this charge transfer transition is no longer observed. The absorption spectra of Al-2Ac and P-3Ac are close to that of AQ, with a slight shift of the π–π* transition in the near-UV region (λ_{max} (P-3Ac) = 335 nm, ε_{335nm} (P-3Ac) = 5870 L mol^{-1} cm^{-1}; λ_{max} (Al-2Ac) = 330 nm, ε_{330nm} (Al-2Ac) = 5750 L mol^{-1} cm^{-1}). Interestingly, Al-2Ac and P-3Ac show significant absorbance up to 500 nm, allowing their use as photosensitizers under visible-light LED irradiation at 405 nm, 455 nm and 470 nm.

Their reactivities alone and their combination with a thiol cross-linker (TT) were also investigated. Steady state photolysis experiments were carried out under LED@405nm irradiation in ACN at room temperature (Fig. S4 and S5† for Al-2Ac and P-3Ac, respectively), while ESR-ST experiments were conducted in DCM in oxygen-free solution in order to identify radical intermediates (Fig. 2, S6,† and Scheme 1). Similar behaviours were observed for both Al-2Ac and P-3Ac in photolysis experiments. Indeed, no photobleaching of P3-Ac (or Al-2Ac) alone was observed even after 10 min of irradiation, thus indicating their stability under light exposure. The irradiation of the oxygen-free P-3Ac/TT/DMPO solution under LED@405 nm led to the generation of one well-resolved ESR signal (Fig. 2). The spin-Hamiltonian parameters elucidated from the simulated spectra (*i.e.*, a_N = 1.37 mT, a_H^β = 1.26 mT, a_H^γ = 0.09 mT, and a_H^γ = 0.09 mT; g = 2.0059 ± 0.0001) are compatible with the thiyl radical DMPO-adduct[38] (species I, Scheme 1), the concentration of which significantly increased beyond that arising from the Forrester–Hepburn mechanism in the control without light (species I′, Scheme 1). This supports a hydrogen atom transfer reaction from TT to P-3Ac. The spectrum obtained with Al-2Ac/TT/DMPO solution shows the same thiyl radical DMPO-adduct (species I, Scheme 1) as the main component (Fig. S6†), superimposed with the product of a secondary spin trapping reaction (*i.e.*, a_N = 1.42 mT; g = 2.0060 ± 0.0001; species II, Scheme 1). Indeed, at a high thiyl radical

DMPO-adduct concentration, the spin adduct disproportionates to the corresponding hydroxylamine and nitrone, which can in turn react with thiyl radicals (inset in Scheme 1). This supports the high rate of formation of thiyl radicals in this system. We performed DFT calculations on the reaction between P3-Ac and TT as well as Al-2Ac and TT. Considering the central reaction in Scheme 1, in which the anthraquinoidic dye is in its lowest triplet state, the formation of the semiquinone radical is strongly thermodynamically favoured with DG of −25 kcal mol^{-1} and −26 kcal mol^{-1} for the alizarin and purpurin derivatives, respectively. In contrast, starting from the ground singlet state of the dye would lead unfavorable reactions by more than 30 kcal mol^{-1}, clearly hinting that excitation of the dye is necessary to initiate the reaction. The molecular modeling is fully consistent with fluorescence experiments: indeed, the emission properties of Al-2Ac and P-3Ac were investigated in diluted acetonitrile or chloroform solutions and did not reveal any fluorescence signals arising from these compounds.

Thiol–ene initiated photopolymerization of terpenes with photosensitizer/TT systems

The formation of thiyl radicals with P-3Ac (or Al-2Ac)/TT photo-initiating systems under visible-light irradiation makes them promising systems for thiol–ene reactions with terpenes. Indeed, terpenes represent a family of plant-extracted components, abundant in nature, offering a wide diversity of structures with carbon double bonds.[49] As a consequence, the capability of P-3Ac (or Al-2Ac)/TT systems to promote the thiol–ene reaction with linalool or geraniol was evaluated. Therefore, we investigated the polymerization of terpene/TT blend mixtures, *i.e.* 50/50, 67/33 and 75/25 wt%/wt%, corresponding to 1.7/1, 3.5/1 and 5.2/1 ene/thiol molar ratios, respectively, in the pres-

Scheme 1 Nature of the radical species trapped by DMPO and resulting from the photolysis of P-3Ac (or Al-2Ac)/TT/DMPO solutions. Forrester–Hepburn reactions and disproportionation reactions of spin adducts resulting in artefactual ESR signals are also presented.

ence of Al-2Ac and P-3Ac as photosensitizers (0.5wt% with respect to the monomer). The resulting "ene" and "thiol" conversions are reported in Table 2 for linalool (and Table S1† for geraniol), and the corresponding kinetic profiles of terpene/TT blend mixtures are displayed in Fig. S7† for linalool and Fig. S8† for geraniol. All the experiments were carried out under air due to the well-known low sensitivity of the thiol–ene reaction toward oxygen inhibition,[60,61] which is especially interesting for low-viscosity formulations such as those involving terpenes.

Interestingly, high "ene" conversions of linalool (>70%) and a high percentage of thiol consumption are reached with the P-3Ac (or Al-2Ac)/TT photo-initiating systems under LEDs@405 and 455 nm irradiation, especially with linalool. Indeed, the thiyl radicals that are generated from the photolysis of P-3Ac (or Al-2Ac)/TT systems (see EPR ST experiments) add to the allyl function of terpenes. For instance, with 25wt%/75wt%, 33wt%/67wt% and 50wt%/50wt% TT/linalool blend mixtures, the thiol groups are almost completely consumed by P-3Ac and Al-2Ac, allowing "ene" conversions higher than 70% under LEDs@405 nm and 455 nm. However, the "ene" conversions are lower with geraniol. In contrast to linalool, both geraniol allyl groups are not terminal and are at least three times substituted, which may decrease their reactivity.[21] Also, the very low viscosity of the geraniol-based formulations and the evaporation of geraniol under light irradiation make the measurement of "ene" conversions difficult. Some experiments

were also carried out with myrcene and farnesene as monomers, but their low viscosity and their evaporation during photopolymerization prevented the monitoring of their reactivity by RT-FTIR.

The high "ene" conversions obtained despite the use of non-stoichiometric amounts of thiols open great perspectives to reduce the need for petro-sourced cross-linkers in thiol–ene reactions. However, despite the high thiol and "ene" conversions, the low viscosity of terpenes did not allow for obtaining a tack-free and solid material. Terpenes should be mixed with a more viscous monomer, such as vegetable oils, to obtain an intermediate viscosity. In the next section, the photo-reactivity of linalool/SOA blend mixtures was studied in detail. Linalool was chosen due to its intrinsic antibacterial properties.

Concomitant thiol–ene and free-radical polymerization of linalool/SOA blend mixtures with P-3Ac (or Al-2Ac)/TT systems

As previously demonstrated, P-3Ac (or Al-2Ac)/TT initiating systems are effective enough to promote thiol–ene reactions with linalool. However, the low viscosity of terpenes when used alone strongly limits their processability to design 3D materials. In contrast, vegetable oils are characterized by a high viscosity that also causes limitations. Therefore, we suggest polymerizing a TT/Lin/SOA 25%/25%/50% (w/w) blend mixture with the use of Al-2Ac and P-3Ac (0.5 wt%) as PSs. Non-modified alizarin (Al) and purpurin (Pur) were used as reference photosensitizers and their reactivities under light

Table 2 Final IR conversions of TT thiol groups and linalool ene groups in TT/Lin blend mixtures with different ratios (25%/75%, 33%/67% and 50%/50% w/w) under air in the presence of Al-2Ac and P-3Ac under LED@405 nm, 455 nm and 470 nm irradiation after 800 s. [PS] = 0.5 wt%. PS = Al-2Ac and P-3Ac

Photo-initiating systems		405 nm	455 nm	470 nm
Al-2Ac/TT25%/Lin75%	SH	100%	96%	np
	Ene	78%	70%	np
Al-2Ac/TT33%/Lin67%	SH	100%	100%	65%
	Ene	81%	79%	45%
Al-2Ac/TT50%/Lin50%	SH	79%	66%	33%
	Ene	100%	94%	76%
P-3Ac/TT25%/Lin75%	SH	95%	96%	61%
	Ene	76%	69%	50%
P-3Ac/TT33%/Lin67%	SH	100%	96%	86%
	Ene	80%	71%	61%
P-3Ac/TT50%/Lin50%	SH	62%	60%	35%
	Ene	96%	94%	67%

np = no polymerization.

irradiation were compared with those of Al-2Ac and P-3Ac. As the influence of the introduction of linalool on the antibacterial properties of the photoinduced materials would be evaluated later on, the photopolymerization of the TT/SOA 25%/75% (w/w) blend mixture (without linalool) but with Al-2Ac and P-3Ac was also studied. The kinetic profiles of TT/Lin/SOA and TT/SOA formulations are, respectively, displayed in Fig. 3 and 4, and the corresponding reference kinetic profiles with the non-modified purpurin and alizarin are reported in Fig. S9 and S10.† The final acrylate, thiol and "ene" conversions after 800 s of irradiation are reported in Table 3.

As can be seen from Table 3, P-3Ac and Al-2Ac based systems show higher initiating efficiency compared with the reference ones (purpurin and alizarin) under LEDs@405, 455, and 470 nm irradiation both under air and in laminate. Indeed, the natural dye systems based on alizarin and purpurin lead to phenolic radicals, which are well-known to be part of the radical scavenging process. The generated phenoxyl radicals are considered as terminating agents, thus inhibiting the growth of the polymer chains.[62] The polymerization of the TT/SOA blend mixture is highly efficient when using P-3Ac and Al-2Ac photosensitizers under LEDs@405 and 455 nm irradiation. The final thiol and acrylate conversions after 800 s of irradiation are higher than 50% under air and in laminate. However, the acrylate double bond conversions are slightly higher than that observed for thiol ones. The highly efficient acrylate conversions are mainly due to a thiol–ene process and albeit to a lesser extent to a free-radical polymerization of SOA. Thiyl radicals formed through the H-abstraction reaction between P-3Ac (or Al-2Ac) and TT are highly reactive toward the acrylate double bonds and lead to a thiol–ene reaction. The carbon-centred radicals generated by the thiol–ene reaction upon visible-light irradiation can initiate the free-radical polymerization of SOA, thus increasing the final acrylate conversions. Meanwhile, the addition of linalool (in TT/Lin/SOA formulation) leads to a slight decrease of the acrylate conver-

sions and an increase of thiol conversions as linalool is also involved in a thiol–ene process. Not surprisingly, the "ene" final conversion of linalool decreases under air as the oxidation of the allyl function of linalool may occur upon light exposure (Scheme S5†). Notably, the thiol–ene reactions occur even under air with Al-2Ac and P-3Ac photo-initiating systems: indeed, the thiyl radicals generated from the H-abstraction reaction between TT and P-3Ac (or Al-2Ac) react with oxygen to form peroxyl radicals, which can subsequently abstract hydrogen from TT to regenerate thiyl radicals.[35]

In the next section, the selected polymerization conditions are those leading to higher conversions in both "ene" and acrylate groups, *i.e.* in laminate and under LED@405 nm irradiation.
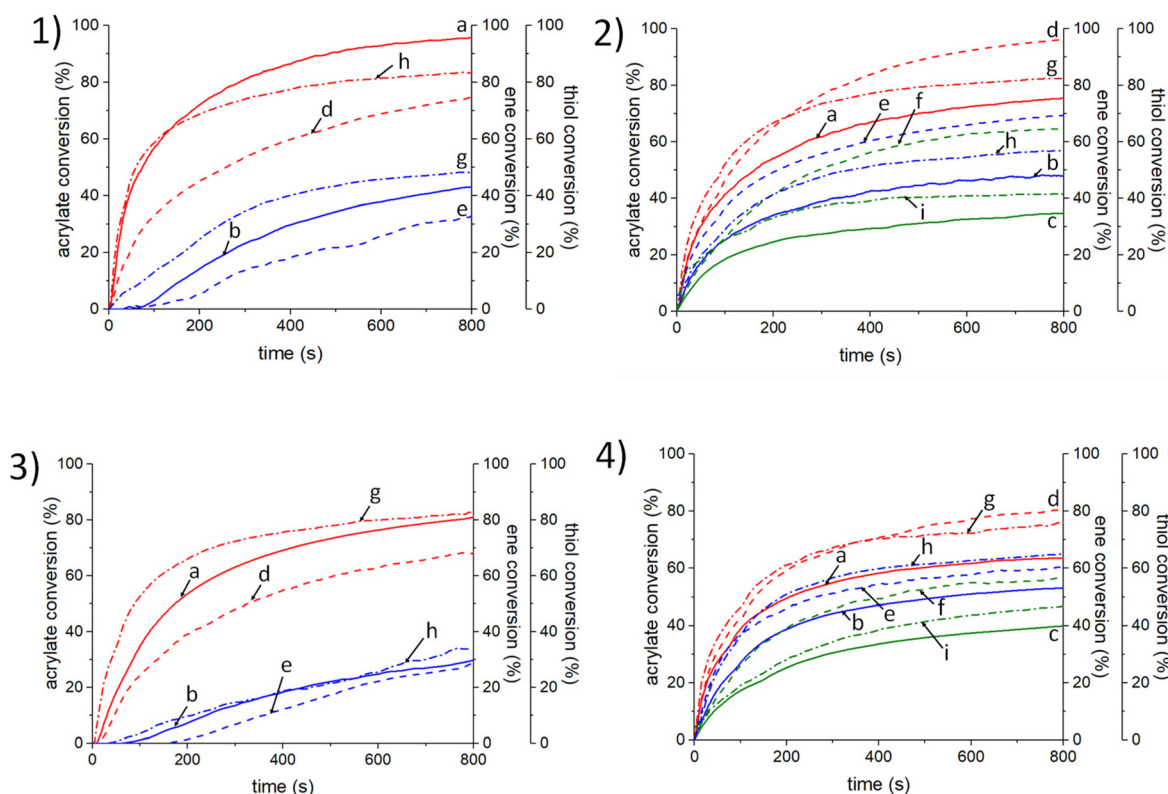
Application of the formulation to the design of high-performing antibacterial materials: selection of the best photosensitizer for the generation of biocide reactive oxygen species (ROS)

Al-2Ac (or P-3Ac) can play a dual role and make the resulting materials photoactive. These photosensitizers can initiate the polymerization when combined with TT as previously demonstrated and can also be used as ROS generators for bacterial inactivation: once trapped in the network, the photosensitizers can be excited again under visible-light exposure and then react with surrounding oxygen to generate ROS. The formation of ROS can occur following two mechanisms.[43,44] The Type I mechanism involves an electron transfer reaction from the dye to oxygen, leading to the formation of reactive oxygen intermediates such as the superoxide ion $O_2^{\cdot-}$, hydrogen peroxide H_2O_2, or hydroxyl radical $HO^{\cdot}$. In the Type II mechanism, an energy transfer process from the excited dye to oxygen leads to the formation of excited oxygen at its singlet state $^1O_2$. Initially, a comparative study was carried out to identify which type of oxygen sensitization mechanism is involved with P-3Ac and Al-2Ac.

Singlet oxygen was detected according to the DPBF method: the oxidation of DPBF in the presence of $^1O_2$ leads to the progressive decrease of its absorbance at 410 nm (Scheme S3†). The superoxide ion was detected using the nitroblue tetrazolium chloride (NB) method by following the increase of the absorbance of the reduced form of NB at 510 nm (Scheme S4†). Each photosensitizer was dissolved in a methanol solution of either DPBF or NB, and the evolution of the UV-vis spectra was monitored over 300 s under xenon lamp irradiation. The results are summarized in Fig. 5A for DPBF and in Fig. 5B for NB. Interestingly, P-3Ac generated singlet oxygen under irradiation, as demonstrated by the fast decrease of DPBF absorbance at 410 nm. However, no singlet oxygen detection was observed for Al-2Ac. These two photosensitizers preferentially react according to a Type I mechanism[63] as the appearance of a strong absorption band between 500 and 570 nm (see Fig. S19†) is assigned to the superoxide anion-derived product of NB.

As singlet oxygen is considered as the most effective biocide agent,[64] P-3Ac is selected as the most promising photosensiti-

230 | *RSC Appl. Polym.*, 2025, **3**, 222–237

© 2025 The Author(s). Published by the Royal Society of Chemistry

Fig. 3 Kinetic profiles of monomer conversions in (1) Al-2Ac/TT25%/Lin25%/SOA50% under air, (2) Al-2Ac/TT25%/Lin25%/SOA50% in laminate, (3) P-3Ac/TT25%/Lin25%/SOA50% under air and (4) P-3Ac/TT25%/Lin25%/SOA50% in laminate: thiol conversion (—) upon (a) LED@405 nm, (b) LED@455 nm and (c) 470 nm irradiation; "ene" conversion (—) upon (d) LED@405 nm, (e) LED@455 nm and (f) LED@470 nm irradiation; and acrylate conversion (-··-) upon (g) LED@405 nm, (h) LED@455 nm and (i) LED@470 nm irradiation. [PS] = 0.5 wt%. PS = Al-2Ac or P-3Ac.

zer to obtain photo-activable materials with antibacterial properties.

Production of singlet oxygen at the surface of the P-3Ac-based materials

Singlet oxygen is a short-lived and highly reactive species.[44] Thus, it is necessary to determine whether the singlet oxygen generated by the irradiation of the P-3Ac-based materials reaches the surface of the pellet. Pellets were synthesized from P-3Ac/TT/SOA and P-3Ac/TT/Lin/SOA formulations under LED@405 nm irradiation. A round silicon mould allowed obtaining homogeneous pellets of 15 mm diameter and 1.3 mm thickness (Fig. S11†). The pellets were immersed in a DPBF solution and irradiated under a xenon lamp. The percentage of the DPBF absorbance over the irradiation time is reported in Fig. 6. Interestingly, the significant decrease of the DPBF absorbance highlights the formation of singlet oxygen at the surface of the pellet. However, a lower amount of singlet oxygen is observed with linalool-containing pellets. This result can be explained by the antioxidant effect of linalool: singlet oxygen may react with the linalool double bond, leading to peroxide derivatives (Scheme S5†).[65] This side reaction partially consumes singlet oxygen generated in P-3Ac/TT/Lin/SOA materials. Nevertheless, a significant amount of singlet oxygen
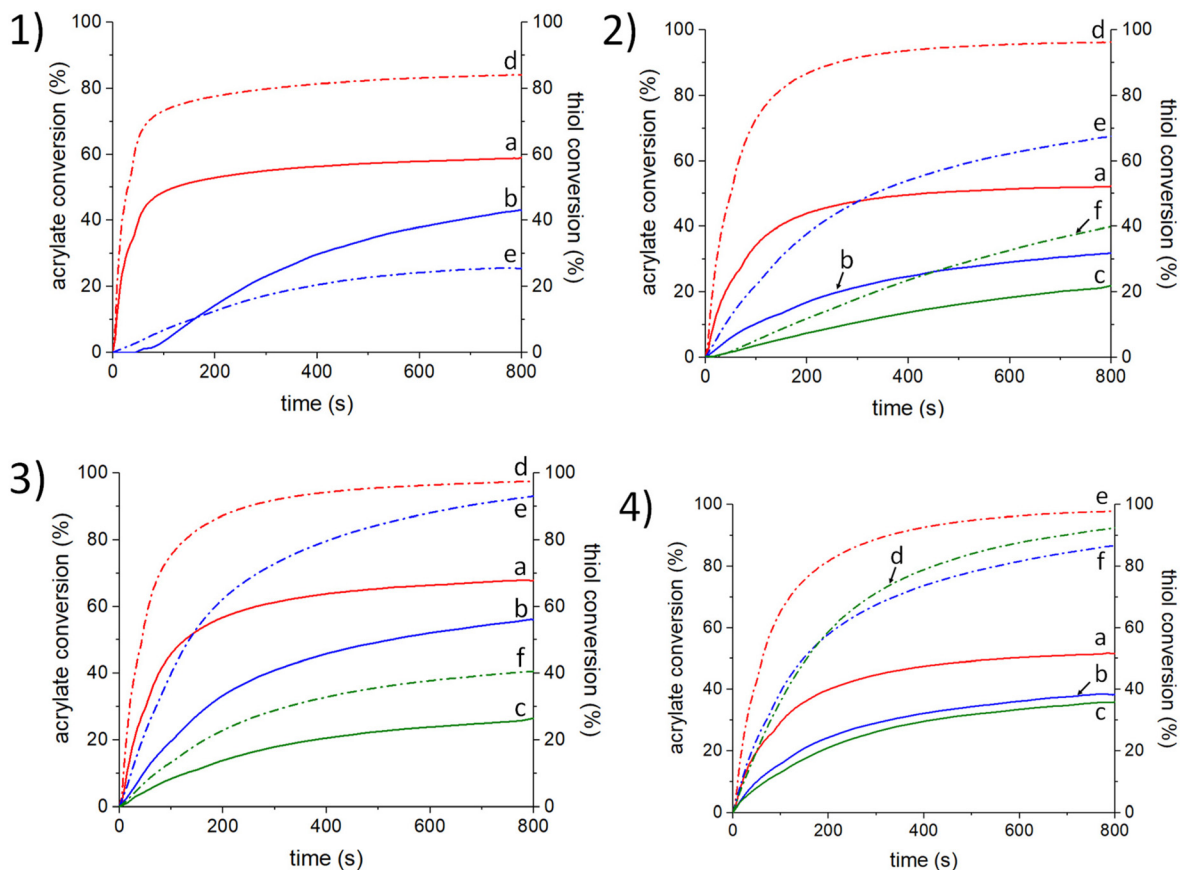
is produced from P-3Ac/TT/Lin/SOA and P-3Ac/TT/SOA materials, suggesting potential photo-activable antibacterial properties.

Antibacterial assay

A dual antibacterial activity is expected for the P-3Ac/TT/Lin/SOA materials according to the antimicrobial properties of linalool and the production of ROS under light irradiation. The combination of both phenomena has antagonistic and synergistic effects against bacteria. The relative contribution of each biocide agent was evaluated against Gram positive (*S. aureus*) and Gram-negative (*E. coli*) bacteria. To maximize bacterial adhesion on the surfaces, the photoinduced materials were put in contact with the bacterial solution for 24 h. The antibacterial properties of the P-3Ac/TT/SOA and P-3Ac/TT/Lin/SOA materials were compared to understand the effect of both visible-light irradiation (under a solar emission lamp) and the presence of linalool on bacterial inhibition (Fig. 7).

Interestingly, a decrease of bacterial adhesion against both *E. coli* and *S. aureus* is observed when linalool is incorporated in the materials. Compared to P-3Ac/TT/SOA samples, 1-log and 2-log reductions of *E. coli* and *S. aureus* adhesion are observed with P-3Ac/TT/Lin/SOA materials without irradiation. Although the mechanism of action of linalool is unknown, its

Fig. 4 Kinetic profiles of acrylate and thiol conversions in (1) Al–2Ac/TT25%/SOA75% under air, (2) Al–2Ac/TT25%/SOA75% in laminate, (3) P–3Ac/TT25%/SOA75% under air and (4) P–3Ac/TT25%/SOA75% in laminate: thiol conversion (—) upon (a) LED@405 nm, (b) LED@455 nm and (c) LED@470 nm irradiation; and acrylate conversion (-··-) upon (d) LED@405 nm, (e) LED@455 nm and (f) LED@470 nm irradiation. [PS] = 0.5 wt%. PS = Al–2Ac or P–3Ac.

antibacterial activity seems to be due to the bacterial membrane disruption after interaction with the linalool hydroxyl group. Besides, the surface hydrophobicity is an important parameter to consider, and a hydrophilic surface tends to decrease bacterial adhesion.[43] Our results are in full agreement with this phenomenon as the P–3Ac/TT/Lin/SOA surface shows a lower water contact angle (60.9°) than that observed without linalool (80.7°, see Table S2†). Consequently, the anti-adhesion properties of linalool-based materials could be attributed either to a contact-killing effect or to a hydrophilic repulsion interaction. Interestingly, the adhesion of *E. coli* on P–3Ac/TT/Lin/SOA surfaces should be unfavourable compared to *S. aureus*, as observed in our experiments, as Gram negative bacterial surfaces are generally more hydrophobic than Gram positive ones.

Also, a strong inhibition of bacteria under solar light exposure can be observed on both materials against *E. coli* and *S. aureus*. For P–3Ac/TT/SOA materials, light exposure leads to a tremendous inhibition of bacterial growth: 99.80% and 99.96% reduction of *S. aureus* and *E. coli*, respectively. The results are similar for both strains, although some previous studies reported that ROS were more virulent against Gram

positive bacteria due to their higher membrane permeability. The inhibition becomes >99.99% for both bacterial strains with P–3Ac/TT/Lin/SOA samples. The synergetic combination of the linalool anti-adhesion effect and ROS production allows this remarkable efficiency. Note that the diffusion of P–3Ac was not observed in bacterial solutions after 24 h of incubation but P–3Ac may have a weak inhibition effect on *E. coli* and *S. aureus* as demonstrated by antibacterial tests in solution (see the ESI, Fig. S12†) when the concentration of P–3Ac is relatively high. In parallel, preliminary cell attachment assays performed using the P–3Ac/TT25%/Lin25%/SOA50% sample showed very poor adhesion of normal human dermal fibroblasts on its surface (Fig. S13†). However, these cells maintained a significant level of metabolic activity compared to the control conditions, suggesting limited cytotoxicity of the sample towards these cells after 24 h.

Reusability of the samples: antibacterial recycling test

Materials were conserved in water for several weeks and reused for a second antibacterial test under similar conditions (Fig. S14†). Compared to the first assay, the antibacterial properties of linalool-based materials dramatically decreased,

232 | *RSC Appl. Polym.*, 2025, **3**, 222–237

© 2025 The Author(s). Published by the Royal Society of Chemistry

Table 3 Final conversions of TT thiol groups, Lin ene groups and SOA acrylate groups in TT/Lin/SOA (25%/25%/50% w/w) and TT/SOA (25%/75% w/w) blend mixtures under air and in laminate in the presence of Al, Al-2Ac, Pur and P-3Ac under LED@405 nm, 455 nm and 470 nm irradiation after 800 s. [PS] = 0.5 wt%. PS = Al, Al-2Ac, Pur and P-3Ac
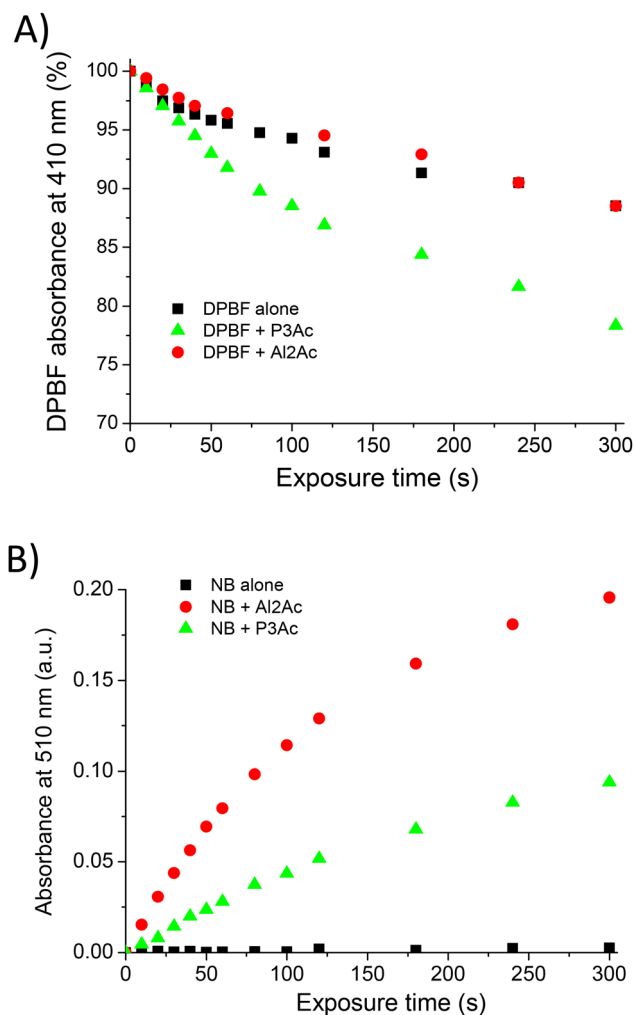
Photo-initiating systems		405 nm		455 nm		470 nm	
		air	lam	air	lam	air	lam
Al/TT25%/Lin25%/	SH	np	69%	np	52%	np	31%
SOA50%	Ene	np	87%	np	73%	np	58%
	Ac	np	76%	np	45%	np	23%
Al-2Ac/TT25%/	SH	97%	77%	45%	51%	np	38%
Lin25%/SOA50%	Ene	76%	99%	34%	73%	np	72%
	Ac	91%	85%	51%	61%	np	46%
Pur/TT25%/Lin25%/	SH	40%	52%	np	30%	np	21%
SOA50%	Ene	56%	71%	np	48%	np	31%
	Ac	52%	61%	np	33%	np	14%
P-3Ac/TT25%/Lin25%/	SH	81%	69%	32%	55%	np	44%
SOA50%	Ene	69%	85%	33%	65%	np	61%
	Ac	87%	82%	46%	68%	np	51%
Al/TT25%/SOA75%	SH	np	36%	np	31%	np	20%
	Ac	np	65%	np	52%	np	28%
Al-2Ac/TT25%/	SH	59%	52%	27%	30%	np	22%
SOA75%	Ac	84%	96%	26%	68%	np	40%
Pur/TT25%/SOA75%	SH	np	32%	np	27%	np	27%
	Ac	np	71%	np	40%	np	39%
P-3Ac/TT25%/SOA75%	SH	70%	53%	57%	38%	26%	38%
	Ac	99%	98%	93%	87%	41%	93%

np = no polymerization and lam = laminate.

respectively, to 54% and 73% against *E. coli* and *S. aureus* in non-irradiated samples. To explain this result, the extractible parts of the P3Ac/Lin/TT/SOA and P3Ac/TT/SOA samples were evaluated in distilled water. The pellets were left for 24 h in PBS and dried under vacuum at 50 °C for 24 h. The weight loss was 8.3 ± 1.9% and 19.2 ± 0.7% for P-3Ac/TT/SOA and P-3Ac/TT/Lin/SOA, respectively. The higher extractible part for linalool-containing materials may indicate that linalool is released in aqueous medium, thus explaining the decrease of antibacterial efficiency of the corresponding materials. Interestingly, the antibacterial effect of ROS generation on P3Ac/TT/SOA materials is still intense with a reduction of bacterial adhesion of 99.58% and 99.98%, respectively, for *E. coli* and *S. aureus* upon light irradiation. For P3Ac/TT/Lin/SOA materials, >99.99% inhibition of *E. coli* and *S. aureus* is observed under solar light irradiation. Therefore, a combination of light and linalool-containing materials leads to highly satisfactory antibacterial properties.

Rheological study and perspectives for 3D-photoprinting of greener materials

As demonstrated above, a bio-based photopolymerizable formulation can lead to high-performing antibacterial materials. In the fight against nosocomial infections, this kind of system could find applications as a coating in medical facilities or as 3D-printable materials. In this context, the processability of the formulation must be discussed. The 3D-printing process requires a viscosity that is sufficiently low to facilitate flow con-
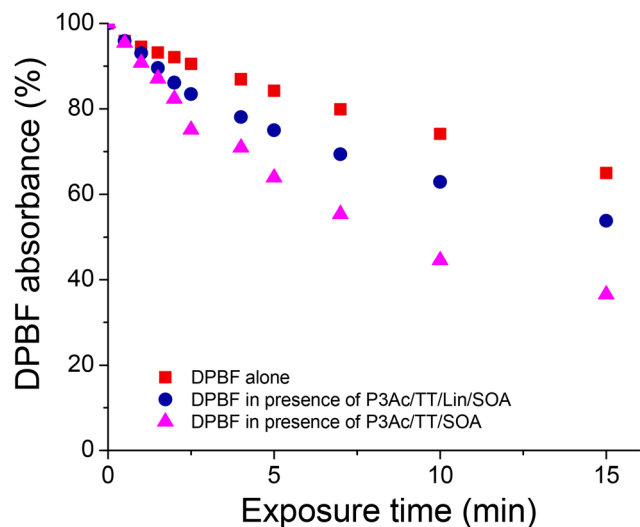

Fig. 5 Detection of (A) singlet oxygen with DPBF and (B) superoxide anion radical with NB using different photosensitizers (PS = P-3Ac and Al-2Ac) under xenon lamp irradiation (10 mW cm^{-2}) in methanol. [DPBF] = 0.03 mM, [NB] = 0.9 mM, and [PS] = 0.3 mM.

tinuity between layers, yet sufficiently high to preserve object integrity. Printable resin viscosities between 0.1 and 10 Pa s are generally reported in the literature and commercial products. It is a limiting factor in the processability of some bio-based monomers by vat polymerization. Notably, viscosities are too low in the case of terpenes (9.07 mPa s at room temperature for linalool, one of the highest among terpenes) and too high in the case of vegetable oils (14 Pa s at room temperature for SOA). Terpenes can hardly be used for 3D-photoprinting without a pre-polymerization step.[21] In the case of SOA, increasing temperature up to 50 °C decreases its viscosity and makes it processable, but requires important energy consumption.[38] Thus, SOA is often diluted with solvents,[26] or synthetic[27] or biobased diluents[13,27] for 3D-printing. The common viscosities of SOA-based 3D printable formulations reported in the literature are between 0.5 and 7.2 Pa s (ref. 66) or 0.14–4.6 Pa s.[27] In this study, linalool is not only used as an antibacterial agent but also as a bio-based monomer and
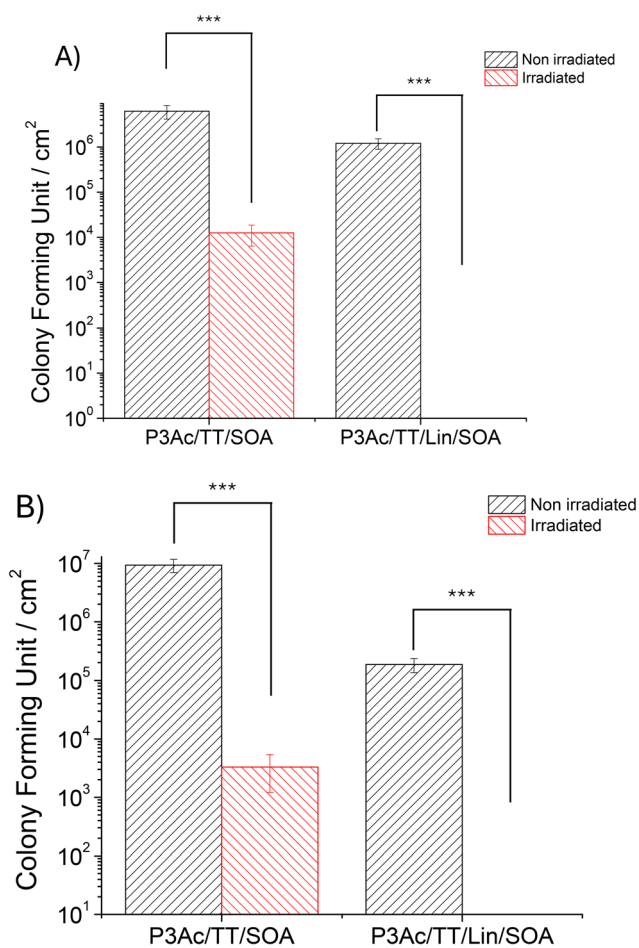
© 2025 The Author(s). Published by the Royal Society of Chemistry

RSC Appl. Polym., 2025, **3**, 222–237 | **233**

Fig. 6 Detection of singlet oxygen production from the irradiation of P-3Ac/TT/Lin/SOA and P-3Ac/TT/SOA pellets with a xenon lamp (10 mW cm^{-2}) in methanol. [DPBF] = 0.03 mM.

Fig. 8 3D photo-printing of a star and a rod with the TT/Lin/SOA (25%/25%/50% w/w) formulation with P-3Ac (0.5 wt%) using DLP technology upon 405 nm light emitting diode exposure. Dimensions of the star: x = 15.129 mm, y = 16.469 mm and z = 2.953 mm. Dimensions of the rod: x = 30.40 mm, y = 9.80 mm and z = 2.58 mm.

Fig. 7 Evolution of the colony forming units (CFUs) of (A) *S. aureus* and (B) *E. coli* at the surface of the P-3Ac/TT/SOA and P-3Ac/TT/Lin/SOA materials with and without visible-light exposure (***p < 0.001).

diluent for SOA. A rheological study of the TT/Lin/SOA (25%/25%/50% w/w) and TT/SOA (25%/75% w/w) formulations was done to evaluate the viscosity as a function of shear rate and temperature (Fig. S15†). Constant viscosities over shear rate sweeps were observed, indicating Newtonian behaviours. For the TT/SOA mixture, a viscosity of 5 Pa s is measured at room temperature but a viscosity nearly half as low is observed with TT/Lin/SOA (1.9 Pa s at room temperature). Therefore, the viscosity of our linalool-based formulations seems sufficient to perform 3D-photoprinting experiments. As a result, DLP experiments with such a formulation were carried out upon 405 nm light emitting diode exposure and 3D objects (*i.e.* a star and a rod) were successfully designed (Fig. 8). It is worth noting that this new formulation not only exhibits excellent antibacterial properties and 3D processability, but also exhibits a high percentage (76%) of bio-renewable carbon content (BCC, calculated from eqn (S1)†).

Conclusions

Two new methacrylate-based hydroxyanthraquinones derived from purpurin and alizarin (P-3Ac and Al-2Ac, respectively) have been designed and used as high-performing visible-light photosensitizers. The combination of P-3Ac (or Al-2Ac) with a thiol crosslinker allows the promotion of the FRP of different acrylate monomers up to 470 nm and demonstrates better initiating properties than those observed with commonly used photosensitizers. The possibility of polymerizing several bio-based monomers, notably vegetable oils (SOA) and terpenes (linalool and geraniol), was also investigated. A bio-based formulation, P-3Ac/TT25%/Lin25%/SOA50%, has been proposed

234 | *RSC Appl. Polym.*, 2025, **3**, 222–237

© 2025 The Author(s). Published by the Royal Society of Chemistry

e

to design materials with dual antibacterial properties, *i.e.* biocide effect in the presence of linalool and photo-activable properties according to the generation of ROS under visible-light irradiation. The combination of these two antibacterial effects leads to a tremendous inhibition of bacterial growth, which remains higher than 99.99% for both *S. aureus* and *E. coli*, even after a second antibacterial recycling test. Interestingly, the purpurin-based formulation (P-3Ac/TT/Lin/SOA), which shows a viscosity in the range of those described for 3D-photoprintable resins at room temperature and which possesses a high bio-renewable carbon content (BCC = 76%), has been successfully used to design 3D objects by the DLP process upon 405 nm light emitting diode exposure.

Author contributions

L. Breloy: data curation, formal analysis, and writing – original draft; C. Elian: data curation; S. Abbad Andaloussi: data curation and validation; S. Lajnef: data curation, formal analysis, methodology, and validation; F. Peyrot: formal analysis, data curation, validation, visualization, methodology, and investigation; V. Alphonse: formal analysis (antibacterial tests in solution) and data curation; S. Pascal: formal analysis (fluorescence data); D. Jacquemin: formal analysis (molecular modelling) and data curation; E. Devernois: formal analysis, investigation, and visualization; T. Coradin: methodology, validation, and writing – review and editing; D.-L. Versace: conceptualization, data curation, formal analysis, funding acquisition, investigation, project administration, supervision, validation, writing – original draft, and writing – review and editing.

Data availability

The data supporting this article have been included as part of the ESI.†

Conflicts of interest

There are no conflicts to declare.

Acknowledgements

References

1 P. C. M. Skoczinski, D. de Guzman, H. Käb, R. Chinthapalli, J. Ravenstijn, W. Baltus and A. Raschka, *Report on the global bio-based polymer market 2020 – A deep and comprehensive insight into this dynamic market*, Nova-Institut GmbH, 2021.

2 M. A. Dubé and S. Salehpour, Applying the Principles of Green Chemistry to Polymer Production Technology, *Macromol. React. Eng.*, 2014, **8**(1), 7–28.

3 L. Pierau, C. Elian, J. Akimoto, Y. Ito, S. Caillol and D.-L. Versace, Bio-sourced monomers and cationic photo-polymerization–The green combination towards eco-friendly and non-toxic materials, *Prog. Polym. Sci.*, 2022, **127**, 101517.

4 Y. Yagci, S. Jockusch and N. J. Turro, Photoinitiated Polymerization: Advances, Challenges, and Opportunities, *Macromolecules*, 2010, **43**(15), 6245–6260.

5 C. Dietlin, S. Schweizer, P. Xiao, J. Zhang, F. Morlet-Savary, B. Graff, J.-P. Fouassier and J. Lalevée, Photopolymerization upon LEDs: new photoinitiating systems and strategies, *Polym. Chem.*, 2015, **6**(21), 3895–3912.

6 A. Bagheri and J. Jin, Photopolymerization in 3D Printing, *ACS Appl. Polym. Mater.*, 2019, **1**(4), 593–611.

7 M. Zanon, R. Cue-López, E. Martínez-Campos, P. Bosch, D.-L. Versace, H. Hayek, N. Garino, C. F. Pirri, M. Sangermano and A. Chiappone, Bioderived dyes-mediated vat photopolymerization 3D printing of chitosan hydrogels for tissue engineering, *Addit. Manuf.*, 2023, **69**, 103553.

8 C. Noe, M. Hakkarainen and M. Sangermano, Cationic UV-Curing of Epoxidized Biobased Resins, *Polymers*, 2020, **13**(1), 89.

9 P. Liu, X. Zhang, R. Liu, X. Liu and J. Liu, Highly functional bio-based acrylates with a hard core and soft arms: From synthesis to enhancement of an acrylated epoxidized soybean oil-based UV-curable coating, *Prog. Org. Coat.*, 2019, **134**, 342–348.

10 S. Ma, Y. Jiang, X. Liu, L. Fan and J. Zhu, Bio-based tetra-functional crosslink agent from gallic acid and its enhanced soybean oil-based UV-cured coatings with high performance, *RSC Adv.*, 2014, **4**(44), 23036.

11 G. Miezinyte, J. Ostrauskaite, E. Rainosalo, E. Skliutas and M. Malinauskas, Photoresins based on acrylated epoxidized soybean oil and benzenedithiols for optical 3D printing, *Rapid Prototyping J.*, 2019, **25**(2), 378–387.

12 C. Wang, L. Ding, M. He, J. Wei, J. Li, R. Lu, H. Xie and R. Cheng, Facile one–step synthesis of bio–based AESO resins, *Eur. J. Lipid Sci. Technol.*, 2016, **118**(10), 1463–1469.

13 M. Lebedevaite, J. Ostrauskaite, E. Skliutas and M. Malinauskas, Photoinitiator Free Resins Composed of Plant-Derived Monomers for the Optical micro-3D Printing of Thermosets, *Polymers*, 2019, **11**(1), 116.

14 S. Molina-Gutierrez, S. Dalle Vacche, A. Vitale, V. Ladmiral, S. Caillol, R. Bongiovanni and P. Lacroix-Desmazes, Photoinduced Polymerization of Eugenol-Derived Methacrylates, *Molecules*, 2020, **25**(15), 3444.

15 C. Noè, S. Malburet, E. Milani, A. Bouvet–Marchand, A. Graillot and M. Sangermano, Cationic UV–curing of epoxidized cardanol derivatives, *Polym. Int.*, 2020, **69**(8), 668–674.

16 L. Pezzana, M. Mousa, E. Malmström, M. Johansson and M. Sangermano, Bio-based monomers for UV-curable coat-

© 2025 The Author(s). Published by the Royal Society of Chemistry

RSC Appl. Polym., 2025, **3**, 222–237 | **235**

ings: allylation of ferulic acid and investigation of photo-cured thiol-ene network, *Prog. Org. Coat.*, 2021, **150**, 105986.

17 C. Noè, S. Malburet, A. Bouvet-Marchand, A. Graillot, C. Loubat and M. Sangermano, Cationic photo-polymerization of bio-renewable epoxidized monomers, *Prog. Org. Coat.*, 2019, **133**, 131–138.

18 M. Firdaus, Thiol-Ene (Click) Reactions as Efficient Tools for Terpene Modification, *Asian J. Org. Chem.*, 2017, **6**(12), 1702–1714.

19 M. Claudino, J.-M. Mathevet, M. Jonsson and M. Johansson, Bringing d-limonene to the scene of bio-based thermoset coatings via free-radical thiol–ene chemistry: macromonomer synthesis, UV-curing and thermo-mechanical characterization, *Polym. Chem.*, 2014, **5**(9), 3245–3260.

20 J. V. Crivello and B. Yang, Studies of synthesis and cationic photopolymerization of three isomeric monoterpene diep-oxides, *J. Polym. Sci., Part A:Polym. Chem.*, 1995, **33**(11), 1881–1890.

21 A. C. Weems, K. R. Delle Chiaie, J. C. Worch, C. J. Stubbs and A. P. Dove, Terpene- and terpenoid-based polymeric resins for stereolithography 3D printing, *Polym. Chem.*, 2019, **10**(44), 5959–5966.

22 S. L. Kristufek, K. T. Wacker, Y. T. Tsao, L. Su and K. L. Wooley, Monomer design strategies to create natural product-based polymer materials, *Nat. Prod. Rep.*, 2017, **34**(4), 433–459.

23 L. Pezzana, E. Malmstrom, M. Johansson and M. Sangermano, UV-Curable, Bio-Based Polymers Derived from Industrial Pulp and Paper Processes, *Polymers*, 2021, **13**(9), 1530.

24 C. Veith, F. Diot-Néant, S. A. Miller and F. Allais, Synthesis and polymerization of bio-based acrylates: a review, *Polym. Chem.*, 2020, **11**(47), 7452–7470.

25 V. S. D. Voet, J. Guit and K. Loos, Sustainable Photopolymers in 3D Printing: A Review on Biobased, Biodegradable, and Recyclable Alternatives, *Macromol. Rapid Commun.*, 2021, **42**(3), e2000475.

26 S. Miao, W. Zhu, N. J. Castro, M. Nowicki, X. Zhou, H. Cui, J. P. Fisher and L. G. Zhang, 4D printing smart biomedical scaffolds with novel soybean oil epoxidized acrylate, *Sci. Rep.*, 2016, **6**, 27226.

27 V. S. D. Voet, T. Strating, G. H. M. Schnelting, P. Dijkstra, M. Tietema, J. Xu, A. J. J. Woortman, K. Loos, J. Jager and R. Folkersma, Biobased Acrylate Photocurable Resin Formulation for Stereolithography 3D Printing, *ACS Omega*, 2018, **3**(2), 1403–1408.

28 A. C. Weems, K. R. Delle Chiaie, R. Yee and A. P. Dove, Selective Reactivity of Myrcene for Vat Photopolymerization 3D Printing and Postfabrication Surface Modification, *Biomacromolecules*, 2020, **21**(1), 163–170.

29 G. Noirbent and F. Dumur, Photoinitiators of polymeriz-ation with reduced environmental impact: Nature as an unlimited and renewable source of dyes, *Eur. Polym. J.*, 2021, **142**, 110109.

30 M. M. Abdul-Monem, Naturally Derived Photoinitiators for Dental and Biomaterials Applications, *Eur. Dent. Res. Biomater. J.*, 2021, **1**(02), 72–78.

31 M. Condat, P. E. Mazeran, J. P. Malval, J. Lalevée, F. Morlet-Savary, E. Renard, V. Langlois, S. Abbad Andaloussi and D. L. Versace, Photoinduced curcumin derivative-coatings with antibacterial properties, *RSC Adv.*, 2015, **5**(104), 85214–85224.

32 X. Peng, D. Zhu and P. Xiao, Naphthoquinone derivatives: Naturally derived molecules as blue-light-sensitive photo-initiators of photopolymerization, *Eur. Polym. J.*, 2020, **127**, 109569.

33 C. Elian, V. Brezová, P. Sautrot-Ba, M. Breza and D. L. Versace, Lawsone Derivatives as Efficient Photopolymerizable Initiators for Free-Radical, Cationic Photopolymerizations, and Thiol-Ene Reactions, *Polymers*, 2021, **13**(12), 2015.

34 P. Sautrot-Ba, V. Brezová, J.-P. Malval, A. Chiappone, L. Breloy, S. Abbad-Andaloussi and D.-L. Versace, Purpurin derivatives as visible-light photosensitizers for 3D printing and valuable biological applications, *Polym. Chem.*, 2021, **12**(17), 2627–2642.

35 P. Sautrot-Ba, S. Jockusch, J.-P. Malval, V. Brezová, M. Rivard, S. Abbad-Andaloussi, A. Blacha-Grzechnik and D.-L. Versace, Quinizarin Derivatives as Photoinitiators for Free-Radical and Cationic Photopolymerizations in the Visible Spectral Range, *Macromolecules*, 2020, **53**(4), 1129–1141.

36 J. Zhang, N. Hill, J. Lalevee, J. P. Fouassier, J. Zhao, B. Graff, T. W. Schmidt, S. H. Kable, M. H. Stenzel, M. L. Coote and P. Xiao, Multihydroxy-Anthraquinone Derivatives as Free Radical and Cationic Photoinitiators of Various Photopolymerizations under Green LED, *Macromol. Rapid Commun.*, 2018, **39**(19), e1800172.

37 J. Zhang, J. Lalevée, J. Zhao, B. Graff, M. H. Stenzel and P. Xiao, Dihydroxyanthraquinone derivatives: natural dyes as blue-light-sensitive versatile photoinitiators of photo-polymerization, *Polym. Chem.*, 2016, **7**(47), 7316–7324.

38 L. Breloy, V. Brezová, Z. Barbieriková, Y. Ito, J. Akimoto, A. Chiappone, S. Abbad-andaloussi, J.-P. Malval and D.-L. Versace, Methacrylated Quinizarin Derivatives for Visible-Light Mediated Photopolymerization: Promising Applications in 3D-Printing Biomaterials, *ACS Appl. Polym. Mater.*, 2022, **4**(1), 210–228.

39 C. J. Cooksey, Quirks of dye nomenclature. 14. Madder: queen of red dyes, *Biotech. Histochem.*, 2020, **95**(6), 474–482.

40 B. Dulo, K. Phan, J. Githaiga, K. Raes and S. De Meester, Natural Quinone Dyes: A Review on Structure, Extraction Techniques, Analysis and Application Potential, *Waste Biomass Valorization*, 2021, **12**(12), 6339–6374.

41 M. Haque, M. Sartelli, J. McKimm and M. Abu Bakar, Health care-associated infections - an overview, *Infect. Drug Resist.*, 2018, **11**, 2321–2333.

42 I. Chiulan, E. B. Heggset, S. I. Voicu and G. Chinga-Carrasco, Photopolymerization of Bio-Based Polymers in a

Biomedical Engineering Perspective, *Biomacromolecules*, 2021, **22**(5), 1795–1814.

43 D.-L. Versace, L. Breloy, E. Palierse and T. Coradin, Contributions of photochemistry to bio-based antibacterial polymer materials, *J. Mater. Chem. B*, 2021, **9**, 9624–9641.

44 C. Elian, R. Méallet and D.-L. Versace, Photoactive Dye-Loaded Polymer Materials: A New Cutting Edge for Antibacterial Photodynamic Therapy, *Adv. Funct. Mater.*, 2024, 2407228.

45 P. Sautrot-Ba, J.-P. Malval, M. Weiss-Maurin, J. Paul, A. Blacha-Grzechnik, S. Tomane, P.-E. Mazeran, J. Lalevée, V. Langlois and D.-L. Versace, Paprika, Gallic Acid, and Visible Light: The Green Combination for the Synthesis of Biocide Coatings, *ACS Sustainable Chem. Eng.*, 2018, **6**(1), 104–109.

46 P. Sautrot-Ba, A. Contreras, S. Abbad Andaloussi, T. Coradin, C. Hélary, N. Razza, M. Sangermano, P. E. Mazeran, J. P. Malval and D. L. Versace, Eosin-mediated synthesis of polymer coatings combining photo-dynamic inactivation and antimicrobial properties, *J. Mater. Chem. B*, 2017, **5**(36), 7572–7582.

47 L. Breloy, V. Brezová, A. Blacha-Grzechnik, M. Presset, M. S. Yildirim, I. Yilmaz, Y. Yagci and D.-L. Versace, Visible Light Anthraquinone Functional Phthalocyanine Photoinitiator for Free-Radical and Cationic Polymerizations, *Macromolecules*, 2019, **53**(1), 112–124.

48 L. Pierau, S. Abbad Andaloussi, A. Chiappone, S. Lajnef, F. Peyrot, J.-P. Malval, S. Jockusch and D.-L. Versace, Eosin Y derivatives for visible light-mediated free-radical polymer-ization: Applications in 3D-photoprinting and bacterial photodynamic inactivation, *Eur. Polym. J.*, 2024, **214**, 113143.

49 C. Elian, S. A. Andaloussi, R. Moilleron, J.-W. Decousser, C. Boyer and D.-L. Versace, Biobased polymer resources and essential oils: a green combination for antibacterial applications, *J. Mater. Chem. B*, 2022, **10**(44), 9081–9124.

50 T. Modjinou, D.-L. Versace, S. Abbad-Andaloussi, V. Langlois and E. Renard, Antibacterial and antioxidant photoinitiated epoxy co-networks of resorcinol and eugenol derivatives, *Mater. Today Commun.*, 2017, **12**, 19–28.

51 L. Breloy, C. A. Ouarabi, A. Brosseau, P. Dubot, V. Brezova, S. Abbad Andalloussi, J.-P. Malval and D.-L. Versace, β-Carotene/Limonene Derivatives/Eugenol: Green Synthesis of Antibacterial Coatings under Visible-Light Exposure, *ACS Sustainable Chem. Eng.*, 2019, **7**(24), 19591–19604.

52 T. Modjinou, D. L. Versace, S. A. Andaloussi, V. Langlois and E. Renard, Co-Networks Poly(hydroxyalkanoates)-Terpenes to Enhance Antibacterial Properties, *Bioengineering*, 2020, **7**(1), 13.

53 T. Modjinou, D.-L. Versace, S. Abbad-Andallousi, N. Bousserrhine, J. Babinot, V. Langlois and E. Renard, Antibacterial Networks Based on Isosorbide and Linalool by Photoinitiated Process, *ACS Sustainable Chem. Eng.*, 2015, **3**(6), 1094–1100.

54 M. B. Kasiri and S. Safapour, Natural dyes and antimicro-bials for green treatment of textiles, *Environ. Chem. Lett.*, 2013, **12**(1), 1–13.

55 M. J. T. Frisch, G. W. Trucks, H. B. Schlegel, G. E. Scuseria, M. A. Robb, J. R. Cheeseman, G. Scalmani, V. Barone, G. A. Petersson, H. Nakatsuji, X. Li, M. Caricato, A. V. Marenich, J. Bloino, B. G. Janesko, R. Gomperts, B. Mennucci, H. P. Hratchian, J. V. Ortiz, A. F. Izmaylov, J. L. Sonnenberg, D. Williams-Young, F. Ding, F. Lipparini, F. Egidi, J. Goings, B. Peng, A. Petrone, T. Henderson, D. Ranasinghe, V. G. Zakrzewski, J. Gao, N. Rega, G. Zheng, W. Liang, M. Hada, M. Ehara, K. Toyota, R. Fukuda, J. Hasegawa, M. Ishida, T. Nakajima, Y. Honda, O. Kitao, H. Nakai, T. Vreven, K. Throssell, J. A. Montgomery Jr, J. E. Peralta, F. Ogliaro, M. J. Bearpark, J. J. Heyd, E. N. Brothers, K. N. Kudin, V. N. Staroverov, T. A. Keith, R. Kobayashi, J. Normand, K. Raghavachari, A. P. Rendell, J. C. Burant, S. S. Iyengar, J. Tomasi, M. Cossi, J. M. Millam, M. Klene, C. Adamo, R. Cammi, J. W. Ochterski, R. L. Martin, K. Morokuma, O. Farkas, J. B. Foresman and D. J. Fox, *Gaussian 16, Revision A.03*, Gaussian, Inc., Wallingford, CT, 2016.

56 C. B. V. Adamo, Toward reliable density functional methods without adjustable parameters: The PBE0 model, *J. Chem. Phys.*, 1999, **110**, 6158–6169.

57 S. Stoll and A. Schweiger, EasySpin, a comprehensive soft-ware package for spectral simulation and analysis in EPR, *J. Magn. Reson.*, 2006, **178**(1), 42–55.

58 J. F. Stanzione 3rd, J. M. Sadler, J. J. La Scala and R. P. Wool, Lignin model compounds as bio-based reactive diluents for liquid molding resins, *ChemSusChem*, 2012, **5**(7), 1291–1297.

59 T. Mukherjee, *Photo and radiation chemistry of quinones*, Indian National Science Academy, India, 2000.

60 A. K. O'Brien, N. B. Cramer and C. N. Bowman, Oxygen inhibition in thiol–acrylate photopolymerizations, *J. Polym. Sci., Part A:Polym. Chem.*, 2006, **44**(6), 2007–2014.

61 N. B. Cramer and C. N. Bowman, Thiol-ene and Thiol-yne Chemistry in Ideal Network Synthesis, in *Thiol–X Chemistries in Polymer and Materials Science*, ed. A. Lowe and C. Bowman, The Royal Society of Chemistry, 2013, pp. 1–27.

62 J. L. Kice, Inhibition of polymerization. II. Methyl acrylate, *J. Polym. Sci.*, 1956, **19**(91), 123–140.

63 H. Görner, Photoreduction of 9,10-anthraquinone deriva-tives: transient spectroscopy and effects of alcohols and amines on reactivity in solution, *Photochem. Photobiol.*, 2003, **77**(2), 171–179.

64 P. Sautrot and D. L. Versace, Photosensitizers as Antibacterial Agents in Polymer Science, in *Photosensitizers: Types, Uses and Selected Research*, ed. C. Whitmire, Nova Science Publisher, 2016.

65 E. M. Elgendy and M. Y. Semeih, Phyto – Monoterpene lina-lool as precursor to synthesis epoxides and hydroperoxides as anti carcinogenic agents via thermal and photo chemical oxidation reactions, *Arabian J. Chem.*, 2019, **12**(7), 966–973.

66 J. Guit, M. B. L. Tavares, J. Hul, C. Ye, K. Loos, J. Jager, R. Folkersma and V. S. D. Voet, Photopolymer Resins with Biobased Methacrylates Based on Soybean Oil for Stereolithography, *ACS Appl. Polym. Mater.*, 2020, **2**(2), 949–957.

© 2025 The Author(s). Published by the Royal Society of Chemistry

RSC Appl. Polym., 2025, **3**, 222–237 | **237**